High-resolution structures of human PLPP3 reveal lipid binding and active-site organization

Yunhai Li[1,2,3#], Cheng-Cen Guo[4#], James Jiqi Wang[5#], Qingning Yuan[1], Jiuyin Xu[1], Zhenyu Cao[6], Xiaoqi Guo[7], Wen Hu[3], Yichao Lin[3], Heng Zhang[3], Yong Li[*2], H. Eric Xu[*1,3,6], Canrong Wu[*1]

https://doi.org/10.15302/vita.2026.11.0092

Dear Editor,

Bioactive lipid phosphates signal from within membranes, yet terminating these signals poses a common challenge for lipid enzymes: a hydrophobic substrate must reach a polar catalytic site at the membrane–water interface. Lysophosphatidic acid (LPA), sphingosine-1-phosphate, and phosphatidic acid are three major classes of bioactive lipids, and they regulate migration, inflammation, endothelial integrity, and vascular remodeling. Phospholipid phosphatases (PLPPs) limit these signals by hydrolyzing their phosphate headgroups[1-4]. Mammalian PLPP1, PLPP2, and PLPP3 share a six-transmembrane fold and conserved catalytic motifs, but PLPP3 is biologically nonredundant. Its loss disrupts vascular development and is linked to coronary artery disease. PLPP3 supports endothelial and vascular homeostasis[5-11]. PLPP3 also partitions into cholesterol- and sphingolipid-enriched membrane domains distinct from those occupied by PLPP1[12,13]. These observations suggest that isoform specificity may be encoded not in the conserved active site, but in the surrounding membrane-facing architecture. We therefore asked how PLPP3 couples bilayer-confined substrate entry to hydrolysis and whether sterols regulate this process.

To address both questions, we determined cryo-electron microscopy (cryo-EM) structures of full-length human PLPP3 in three states: a cholesterol hemisuccinate (CHS)-bound apo state at 1.98 Å, a CHS-containing LPA-incubated state at 2.28 Å, and an apo state prepared without added CHS at 1.97 Å (Fig. 1; Supplementary Figs. S1–S4 and Table S1). Independent C1 and C4 refinements converged on the same compact tetramer under these detergent conditions (Supplementary Figs. S2, S3). Beyond the conserved PLPP fold[3,4,14], the two sub-2-Å reconstructions resolve side-chain rotamers, individual solvent peaks, and ordered lipid- and sterol-associated densities with near-atomic clarity (Fig. 1b; Supplementary Fig. S4). Direct protein contacts establish the tetrameric geometry, while reproducible lipid-like densities fill membrane-facing grooves between protomers (Fig. 1c). Interface-associated substitutions reduce activity (Supplementary Fig. S5), supporting the functional importance of these regions without establishing a requirement for tetramerization.

The structures reveal an extensively hydrated catalytic chamber. Hundreds of ordered water molecules populate the extracellular/luminal loops, internal cavities, and membrane-proximal regions (Supplementary Fig. S1a–c). Discrete solvent densities surround the conserved polar and basic residues and phosphate-binding region (Fig. 1a–c), showing that water is an integral component of the active-site architecture. This hydrated chamber provides the polar environment needed for phosphotransfer while remaining directly connected to the bilayer (Fig. 1c). An ordered water molecule adjacent to H251 is a candidate for hydrolysis of the phosphohistidine intermediate in the conserved PAP2 mechanism, in which H251 acts as the nucleophile and H199 supports acid-base catalysis[3].

The structures also trace a route from the membrane to the catalytic chamber. PLPP3 converts LPA or phosphatidic acid (PA) to monoacylglycerol (MAG) or diacylglycerol (DAG) respectively, with release of inorganic phosphate (Pi) (Fig. 1a). The product-compatible state links that access route to the chemistry that it feeds. Pi sits in the catalytic chamber within a polar and basic network of K148, R155, S197, R245, and H251, with H199 positioned for acid-base catalysis and E190 located just outside this network (Fig. 1c, e). Alanine substitution of any of these residues except E190 reduces phosphate release to the level of the assay control; E190A retains partial activity, indicating that E190 contributes to active-site organization but is not strictly required for catalysis (Fig. 1f). The close alignment of these side chains across all three states is consistent with lipid accommodation and phosphotransfer within a largely preorganized scaffold, without requiring a large-scale conformational transition (Fig. 1d, e).

The three structures resolve sterol at three distinct positions, which differ in their occupancy across states (Fig. 1c). Two lie within the membrane-access pocket: the first sterol, CHS-1, sits at the entrance from the bilayer, and the second sterol, CHS-2, is located in an adjacent recess, with its sterol scaffold directed toward the catalytic chamber; the hemisuccinate moiety is not well resolved (Fig. 1c). In the LPA-incu-

1. Research Center for Medicinal Structural Biology, National Research Center for Translational Medicine at Shanghai, State Key Laboratory of Medical Genomics, Ruijin Hospital affiliated to Shanghai Jiao Tong University School of Medicine, Shanghai, China. 2. State Key Laboratory of Cellular Stress Biology, School of Life Sciences, Xiamen University, Xiamen, Fujian, China. 3. State Key Laboratory of Drug Research, Shanghai Institute of Materia Medica, Chinese Academy of Sciences, Shanghai, China. 4. NHC Key Laboratory of Digestive Diseases (Renji Hospital, Shanghai Jiao Tong University School of Medicine), Division of Gastroenterology and Hepatology, State Key Laboratory for Oncogenes and Related Genes, Renji Hospital, School of Medicine, Shanghai Jiao Tong University, Shanghai, China. 5. Division of Cardiology, Department of Internal Medicine and Hubei Key Laboratory of Genetics and Molecular Mechanism of Cardiologic Disorders, Tongji Hospital, Tongji Medical College, Huazhong University of Science and Technology, Wuhan, Hubei, China. 6. Nanjing University of Chinese Medicine, Nanjing, Jiangsu, China. 7. School of Pharmacy, Nanjing Medical University, Nanjing, Jiangsu, China. #These authors contributed equally. *Correspondence: Yong Li (yongli@xmu.edu.cn), H. Eric Xu (eric.xu@simm.ac.cn), Canrong Wu (wcr13215@rjh.com.cn)

Received: August 7, 2026; Accepted: November 12, 2026; Published: November 20, 2026

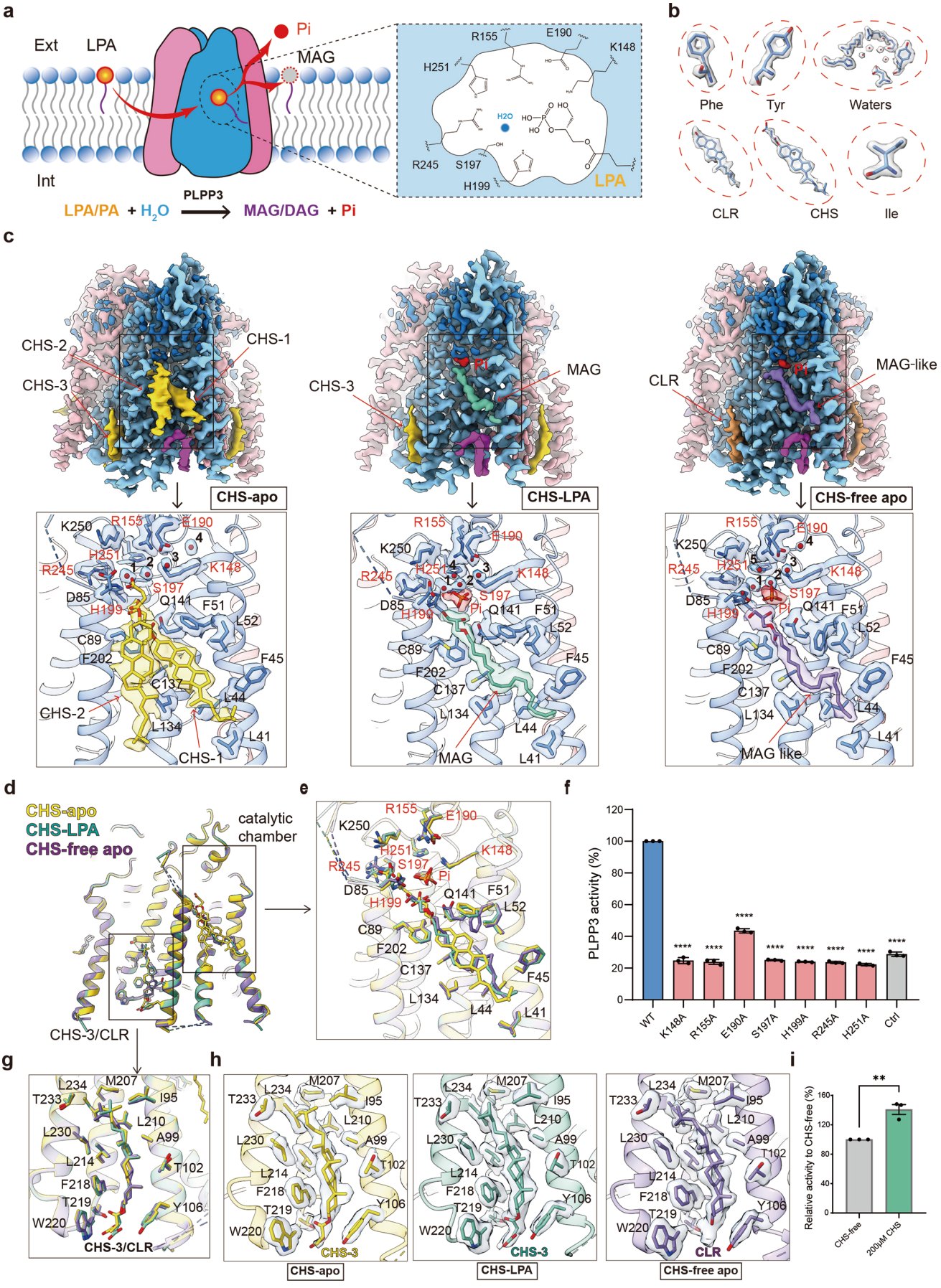

a
Ext
LPA
Pi
MAG
Int
PLPP3
LPA/PA + H2O
MAG/DAG + Pi
R155
E190
K148
H251
H2O
R245
S197
H199
LPA
b
Phe
Tyr
Waters
CLR
CHS
Ile
c
CHS-2
CHS-1
CHS-3
CHS-apo
Pi
MAG
CHS-LPA
MAG-like
CLR
CHS-free apo
K250
R155
E190
H251
R245
K148
S197
D85
H199
Q141
F51
L52
C89
F202
F45
C137
L44
L134
L41
MAG like
d
CHS-apo
CHS-LPA
CHS-free apo
catalytic chamber
CHS-3/CLR
e
f
PLPP3 activity (%)
WT
K148A
R155A
E190A
S197A
H199A
R245A
H251A
Ctrl
g
h
i
Relative activity to CHS-free (%)
CHS-free
200uM CHS

Fig. 1 Near-atomic structures reveal membrane access, hydrated catalysis, and CHS-associated activity changes of human PLPP3. **a** Schematic of PLPP3-catalyzed hydrolysis of LPA or PA to MAG or DAG, respectively, with release of inorganic phosphate (Pi). The inset illustrates the polar catalytic chamber formed by K148, R155, S197, H199, R245, H251, and E190, together with a schematically positioned reaction water molecule. Ext and Int denote the extracellular/luminal and intracellular/cytoplasmic sides, respectively. **b** Representative local cryo-EM densities demonstrating near-atomic map quality, including Phe, Tyr, Ile, ordered water molecules, cholesterol-like density (CLR), and cholesterol hemisuccinate (CHS). **c** Cryo-EM maps and enlarged views of the membrane-access and catalytic regions of CHS-bound apo PLPP3 (CHS-apo; 1.98 Å), CHS-containing LPA-incubated PLPP3 (CHS-LPA; 2.28 Å), and apo PLPP3 prepared without added CHS (CHS-free apo; 1.97 Å). In the CHS-apo structure, CHS-1 occupies the membrane-entry channel, CHS-2 lies in an adjacent recess, and CHS-3 occupies a lateral sterol pocket. In the LPA-incubated product-compatible state, CHS-1 and CHS-2 are absent, MAG occupies the CHS-1-associated access route, and Pi is resolved in the catalytic chamber, whereas CHS-3 remains bound. The structure prepared without added CHS contains a MAG-like density in the access pocket, Pi in the catalytic chamber, and CLR at the lateral CHS-3-equivalent site. Catalytic-network residues are labeled in red. Ordered water molecules are numbered; W1 is a candidate water for phosphohistidine hydrolysis. **d** Superposition of the three PLPP3 structures, showing the conserved overall architecture and the spatial relationship between the catalytic chamber, membrane-access region, and persistent lateral CHS-3/CLR site. **e** Enlarged structural overlay of the catalytic chamber and membrane-access pocket. The phosphate-coordinating and catalytic residues remain closely aligned among the three states, consistent with ligand accommodation within a preorganized catalytic scaffold. **f** LPA phosphatase activities of WT PLPP3 and the indicated catalytic-network mutants, normalized to WT. Substitution of K148, R155, S197, H199, R245, or H251 markedly reduces activity, whereas E190A retains partial activity. Ctrl denotes the matched assay control. **g** Enlarged superposition of the persistent lateral sterol-binding site, showing the overlapping positions of CHS-3 and CLR and the surrounding hydrophobic residues. **h** Individual views of the lateral sterol pocket in the CHS-apo, CHS-LPA, and CHS-free apo structures, containing CHS-3, CHS-3, and CLR, respectively. **i** Relative LPA phosphatase activity of PLPP3 purified without added CHS in the absence or presence of 200 μM CHS. Addition of CHS increases PLPP3 activity by approximately 42%. Data in **f** and **i** are mean ± SEM from three independent measurements. In **f**, statistical significance relative to WT was assessed by one-way ANOVA followed by Dunnett's multiple-comparisons test; in **i**, groups were compared using an unpaired two-tailed Student's *t*-test. $^{**}P < 0.01$; $^{****}P < 0.0001$.

bated structure both sterol densities are absent, a density modeled as MAG occupies the CHS-1 channel, and no ligand is modeled in the CHS-2 recess (Fig. 1c). Proximity to the active site is therefore not sufficient for stable sterol occupancy. The third position behaves differently. A lateral pocket, distinct from the access route, is sterol-occupied in all three preparations: CHS-3 is resolved there in both CHS-containing structures, and an overlapping CLR occupies the same site in the structure prepared without added CHS (Fig. 1g, h). This persistent site is distinct from the substrate access route and is a candidate for sterol-dependent regulation; its contribution to the CHS effect remains untested.

The overlapping positions of CHS-1 and MAG within the substrate-access route prompted us to investigate whether CHS affects PLPP3 activity. Using protein purified without added CHS and matched LMNG vehicle controls, we found that 200 μM CHS unexpectedly enhanced, rather than suppressed, phosphate release: LPA and PA hydrolysis increased by approximately 42% and 35%, respectively ($n = 3$ independent measurements; Fig. 1i; Supplementary Fig. S6; absolute wild-type (WT) specific activities are reported in the Supplementary Information). This consistent enhancement across two substrates demonstrates a reproducible biochemical effect of CHS under the tested detergent conditions. One possible explanation is that exchangeable sterol occupancy in the access region and favorable lateral interactions that affect local packing have different functional consequences. Their net effect could enhance activity despite transient restriction of substrate access, although the contribution of each site remains unproven.

These results support a structural framework for PLPP3 function. PLPP3 assembles into a tetramer associated with ordered lipid under these conditions, and accommodates lipids in a shared sterol/acylglycerol pocket. Hydrolysis occurs in a preorganized, water-rich chamber. Its phosphate-binding region and membrane-facing cavity can accommodate a shared headgroup and different acyl-chain configurations, providing a basis for LPA/PA promiscuity[2-4]. The catalytic residues resolved here are essentially superimposable on those of PLPP1 and PLPP2[3,4], whereas the lipid-facing surfaces and their bound ligands differ markedly. These differences may contribute to lipid recognition. The less conserved interface may offer sites for isoform-selective binding. The genetic association of the PLPP3 locus with coronary artery disease provides a rationale for defining its lipid-binding and catalytic architecture, which may inform future investigations of its vascular functions[6,7]. The high-resolution structures define lipid-binding and hydration features, while CHS-associated activity changes provide a basis for further mechanistic investigation.

DATA AVAILABILITY

The cryo-EM density maps and atomic coordinates of human PLPP3 have been deposited in the Electron Microscopy Data Bank (EMDB) and the Protein Data Bank (PDB), respectively: CHS-bound apo PLPP3 (EMD-85000; PDB 47ZH), CHS-containing LPA-incubated PLPP3 (EMD-84998; PDB 47ZF), and apo PLPP3 prepared without added CHS (EMD-84999; PDB 47ZG). These accession codes are listed in Supplementary Table S1. Supporting biochemical data are presented in the main text and Supplementary Information. The software used for data processing and analysis is described in the Supplementary Information.

ACKNOWLEDGMENTS

The cryo-EM data were collected at the Shanghai Advanced Center for Electron Microscopy, Shanghai Institute of Materia Medica, Chinese Academy of Sciences. This work was supported by the National Natural Science Foundation of China (32301016 to C.W.; 825B2010 to J.J.W.; 32130022, 82495184 and 82121005 to H.E.X.); the National Key R&D Program of China (2022YFC2703105 to H.E.X.); the National Key R&D Program "Strategic Scientific and Technological Innovation Cooperation" Key Project (2022YFE0203600); the CAS Strategic Priority Research Program (XDB37030103 to H.E.X.); the Shanghai Municipal Science and Technology

Major Project (2019SHZDZX02 to H.E.X.); and the Strategic Priority Research Program of the Chinese Academy of Sciences (XDB0830000 to H.E.X.).

AUTHOR CONTRIBUTIONS

Y.H.L., C.-C.G., J.J.W., and C.W. conceived and designed the study. Y.H.L. performed protein expression and purification and prepared cryo-EM samples. Y.H.L. and J.J.W. processed the cryo-EM data and determined the structures. Y.H.L., C.-C.G., Q.Y., J.X., Z.C., X.G., W.H., Y.C.L., and H.Z. performed the biochemical experiments and analyzed the data. Y.H.L., C.-C.G., J.J.W., C.W., and H.E.X. interpreted the structural and functional findings. Y.H.L., C.W., and H.E.X. wrote the manuscript with contributions from all authors. Y.L., C.W., and H.E.X. supervised the research.

COMPETING INTERESTS

The authors declare no competing interests.

REFERENCES

1. Chun, J., Hla, T., Lynch, K.R., Spiegel, S. & Moolenaar, W.H. *Pharmacol. Rev.* **62**, 579–587 (2010).
2. Sigal, Y.J., McDermott, M.I. & Morris, A.J. *Biochem. J.* **387**, 281–293 (2005).
3. Yang, M., Sun, C.P., He, Y.L. & Qian, H.W. *Nat. Chem. Biol.* **22**, 793–801 (2026).
4. Wang, W.Y., Xu, Y., Guo, P.L., Han, H. & Han, L. *Structure* **34**, 955–962.e3 (2026).
5. Escalante-Alcalde, D. et al. *Development* **130**, 4623–4637 (2003).
6. Schunkert, H. et al. *Nat. Genet.* **43**, 333–338 (2011).
7. Reschen, M.E. et al. *PLoS Genet.* **11**, e1005061 (2015).
8. Wu, C.Q. et al. *Circ. Res.* **117**, e41–e53 (2015).
9. Touat-Hamici, Z. et al. *Cardiovasc. Res.* **112**, 702–713 (2016).
10. Chabowski, D.S. et al. *J. Physiol.* **601**, 469–481 (2023).
11. Mueller, P.A. et al. *Arterioscler. Thromb. Vasc. Biol.* **39**, 2261–2272 (2019).
12. Jia, Y.J., Kai, M., Wada, I., Sakane, F. & Kanoh, H. *FEBS Lett.* **552**, 240–246 (2003).
13. Kai, M. et al. *J. Biochem.* **140**, 677–686 (2006).
14. Wu, Y.J. et al. *Nat. Commun.* **17**, 8823 (2026).

ADDITIONAL INFORMATION

Supplementary information The online version contains supplementary material available at https://doi.org/10.15302/vita.2026.11.0092.

Correspondence and requests for materials should be addressed to Yong Li, H. Eric Xu or Canrong Wu.

Reprints and permission information is available at https://www.vita-journal.com/.

© The Author(s) 2026. Published by Higher Education Press. This is an Open Access article distributed under the terms of the CC BY license (https://creativecommons.org/licenses/by/4.0/).